One Phase vs Two-Phase Modelling of Infiltration Processes

Mauro Aimar[1]([envelope]) [iD], Gabriele Della Vecchia[2] [iD], and Guido Musso[1] [iD]

[1] Politecnico di Torino, Corso Duca degli Abruzzi 24, 10129 Turin, Italy
`mauro.aimar@polito.it`

[2] Politecnico di Milano, Piazza Leonardo da Vinci 32, 20133 Milan, Italy

Abstract. Because of global warming, the frequency and harmfulness of climate extreme meteorological events have increased and are expected to increase. Events such as droughts, heatwaves, storms, floodings strongly impact the functioning of critical infrastructure, as well as the stability and degradation of man-made earthworks and natural slopes. The shallower portions of natural soils and earthworks are thus exposed to increasingly severe dry and hot seasons and to intense rainfalls, which affect the depth of the water table and the hydraulic circulation, triggering material degradation and instabilities. Robust modelling of the soil-atmosphere interaction, correctly accounting for unsaturated flow and boundary conditions, is a requirement of modern geotechnical engineering. The assumptions made when modelling infiltration, in terms of infiltration rate, pore and air pressure distribution and evolution, have in fact a relevant impact on model predictions. As a fraction of the pore space of unsaturated soils is occupied by the gas phase, composed of water vapour and dry air, a complete model of infiltration requires accounting for the inflow of the liquid phase and the outflow of the gas phase. Contrarily, infiltration is very often modelled accounting only for the inflow of liquid water. This work explores the consequences and limitations of such simplification by comparing the predictions obtained by adopting both a two-phase and a one-phase model for the simulation of the infiltration processes.

Keywords: Unsaturated soil mechanics · Infiltration · Multi-phase flow

1 Introduction

Global warming is pushing the weather towards increasingly extreme conditions, with severely dry and hot seasons and intense rainfall events. Such phenomena are expected to impact on the hydro-mechanical state of the shallower portions of soil deposits and geotechnical earthworks. Strong evaporation due to dry seasons might end up altering the integrity of earthworks through the occurrence of drying cracks [1], or reduce the effectiveness of cut-off walls [2]. Rainfall and infiltration lead to an increase in the pore water pressure and in the degree of saturation of the slopes, which favor the onset of instabilities [3]. In particular, in the vadose zone – i.e., the shallower portion of soil deposits resting above the water table – the soil is often unsaturated and the pore water pressure is negative (smaller than atmospheric pressure). Its value is controlled

by the interaction between the soil surface and the atmosphere, through evaporation and infiltration, and by the soil hydraulic properties (see, e.g., [4]).

As for infiltration processes, classical modelling approaches only consider the mass transfer of liquid water, whereas no water vapour is accounted for and pore air pressure is assumed as atmospheric (e.g., Richards' equation [5]). However, several studies demonstrated that air entrapment affects the infiltration rate, entailing slower variation in pore water pressure [6–8]. This delay in the pore water pressure increase can be crucial for rainfall-induced slope stability issues, as it may prevent reaching the critical value during the rainfall event. Besides, to the Author's knowledge, the role of water vapour in the infiltration process has not been clearly highlighted yet. This contribution proposes a hydraulic model aimed at reproducing infiltration processes in geomaterials, including the liquid and gas flow of water and air, in order to investigate the influence of water vapour and pore air pressure. Numerical simulations have been performed considering distinct scenarios, including (i) the flow of liquid water only, (ii) both liquid water and water vapour, and (iii) the combined flow of water and air. Model predictions are compared with the transient infiltration problem discussed in Siemens et al. [7].

2   Modelling Water and Air Transport in Unsaturated Soils

Modelling isothermal hydro-mechanical processes in unsaturated soils requires accounting for the linear momentum balance of the solid skeleton and the mass balance of air and water. However, as a first approximation limited to soils whose deformation upon wetting is small (e.g., coarse soils and non-active clays), the linear momentum balance of the solid skeleton can be neglected when modelling infiltration. While the classical description of hydro-mechanical processes is usually performed in terms of fluid phases (*i.e.* liquid and gas), in this study mass balance equations were rather written in terms of chemical species [9].

The mass balance equation for the species water is written by combining the contribution of liquid water and water vapour:

$$\frac{\partial}{\partial t}\left[\phi\left(S_l\rho_l^w + S_g\rho_g^w\right)\right] + \nabla\cdot\left(\rho_l^w\mathbf{q}_l + \rho_g^w\mathbf{q}_g\right) + \nabla\cdot\left[\phi\left(S_l\mathbf{J}_l^w + S_g\mathbf{J}_g^w\right)\right] = 0 \quad (1)$$

where ϕ is porosity, S_l is degree of saturation of the liquid phase, $S_g = 1 - S_l$ is degree of saturation of the gas phase, ρ_l^w is the mass density of the water in the liquid phase, ρ_g^w is the mass density of the water in the gas phase, $\mathbf{q}_l$ is the advective flux of the liquid phase, $\mathbf{q}_g$ is the advective flux of the gas phase, $\mathbf{J}_l^w$ is the diffusive flux of the water in the liquid phase, $\mathbf{J}_g^w$ is the diffusive flux of the water in the gas phase.

The mass balance equation for the species air is written according to a similar formulation:

$$\frac{\partial}{\partial t}\left[\phi\left(S_l\rho_l^a + S_g\rho_g^a\right)\right] + \nabla\cdot\left(\rho_l^a\mathbf{q}_l + \rho_g^a\mathbf{q}_g\right) + \nabla\cdot\left[\phi\left(S_l\mathbf{J}_l^a + S_g\mathbf{J}_g^a\right)\right] = 0 \quad (2)$$

where ρ_l^a is the mass density of the air dissolved in the liquid phase, ρ_g^a is the mass density of the air in the gas phase, $\mathbf{J}_l^a$ is the diffusive flux of the air dissolved in the liquid phase, $\mathbf{J}_g^a$ is the diffusive flux of the air in the gas phase.

The water retention curve provides the link between the degree of saturation S_l and matric suction s, defined as the difference between the pressure of the gas phase p_g and the one of the liquid phase p_l:

$$s = p_g - p_l \tag{3}$$

The liquid density ρ_l^w is assumed to be constant and equal to 1,000 kg/m^3, while the vapour density ρ_g^w has been obtained through the psychrometric law, as a function of the total suction ψ and the partial pressure of water vapour at saturation $p_{g,sat}^w$ (e.g., [10]):

$$\rho_g^w = \frac{p_{g,sat}^w}{RT} \exp\left(-\frac{\Psi M_w}{\rho_l^w RT}\right), \quad p_{g,sat}^w = 0.6108[kPa] \times 10^{\frac{7.5T[°C]}{T[°C]+273.3}} \tag{4}$$

where $R = 8.3145$ J/(mol $\times$ K) is the constant of perfect gases, $M_w = 0.018$ kg/mol is the molar mass of the water, and T is the temperature. For the sake of simplicity, the contribution of the osmotic suction is assumed to be negligible, hence ψ equals s. The gaseous air density $\rho_g{}^a$ is estimated through the law of perfect gases, as a function of the corresponding partial pressure $p_g{}^a$:

$$\rho_g^a = \frac{M_a}{RT} p_g^a \tag{5}$$

The mass density of the air dissolved in the liquid phase $\rho_l{}^a$ is calculated as a function of the liquid water pressure, by means of the Henry's law:

$$\rho_l^a = H\frac{M_a}{RT} p_l^w \tag{6}$$

where $H = 0.031$ is the Henry constant for air dissolved in water.

The advective flux $\mathbf{q}_\alpha$ (with $\alpha = l, g$) can be described through the generalized Darcy law:

$$\mathbf{q}_\alpha = -\mathbf{K}_\alpha \nabla\left(\frac{p_\alpha}{\rho_\alpha g} + h_z\right) \tag{7}$$

where $\mathbf{K}_\alpha$ is the unsaturated hydraulic conductivity tensor, ρ_α is the mass density of the α-phase, and h_z is the elevation head. In isotropic, partially saturated soils, $\mathbf{K}_\alpha$ is an isotropic tensor with magnitude K_α, which can be decomposed into the product between a saturated value $K_{\alpha,sat}$ and a relative permeability coefficient $k_{\alpha,rel}$, dependent on S_α [11].

Instead, the diffusive flux $\mathbf{J}_\alpha{}^\gamma$ (with $\gamma = w, a$) can be predicted through the Fick's law:

$$\mathbf{J}_\alpha^\gamma = -\mathbf{D}_\alpha^\gamma \nabla \rho_\alpha^\gamma \tag{8}$$

where $\mathbf{D}_\alpha{}^\gamma$ is the diffusion tensor of the α-phase of the γ-species in the porous medium. This tensor can be written as follows:

$$\mathbf{D}_\alpha^\gamma = D_\alpha^\gamma \tau_\alpha \tag{9}$$

where $D_\alpha{}^\gamma$ is the diffusion coefficient of the α-phase of the γ-species in "free" conditions, and $\boldsymbol{\tau}_\alpha$ is the tortuosity tensor, which models the tortuosity of the path described by the γ-molecules in the diffusion process. In isotropic, partially saturated soils, $\boldsymbol{\tau}_\alpha$ can be described as an isotropic tensor with magnitude τ_α [12]:

$$\tau_\alpha = (\phi S_\alpha)^{\frac{2}{3}} \tag{10}$$

For the water species, $\mathbf{J}_l{}^w = \mathbf{0}$ due to the assumed constant $\rho_l{}^w$, whereas the diffusion coefficient of the water vapour in free air $D_g{}^w$ is [13]:

$$D_g^w = 0.229 \times 10^{-4} \left[m^2/s \right] \left(1 + \frac{T[K]}{273} \right)^{1.75} \tag{11}$$

As for the air, $\mathbf{J}_g{}^a$ represents the air self-diffusivity and it is assumed to be negligible, whereas the diffusion coefficient of dissolved air in water is $D_l{}^a = 2 \times 10^{-9}$ m^2/s [14]. In this study, the infiltration process is simulated considering three distinct models:

- Model "W_l": only liquid water is included, whereas air remains at atmospheric pressure. In this case, only the mass balance of water is used (Eq. 1), with vapour pressure and density set equal to 0.
- Model "W_{lg}": the mass balance of both liquid water and water vapour is considered (Eq. 1), whereas the mass balance of air is neglected.
- Model "$W_{lg} + A_{lg}$": both water and air species are included, and the full set of equations is implemented.

3   Numerical Model

The hydraulic model is used to address the influence of water vapour and dry air on infiltration processes, with reference to the physical and numerical study presented in Siemens et al. [7], who studied the infiltration of an oil along a vertical column filled with a coarse-grained, isotropic transparent soil, with porosity $\phi = 0.5$. The water retention curve of the soil can be described by the Van Genuchten relationship [15]:

$$S_l = S_{l,r} + \frac{1 - S_{l,r}}{\left[1 + (s/P)^n \right]^m} \tag{12}$$

with $S_{l,r} = 0.03$, $P = 0.17$ kPa, $n = 6.17$, and $m = 0.84$ [6]. The saturated hydraulic conductivity for the liquid and gas phase are $k_{l,sat} = 10^{-3}$ m/s and $k_{g,sat} = 8 \times 10^{-3}$ m/s, while the corresponding relative permeabilities are shown in Fig. 1 as a function of S_l and S_g. The soil column is 1,120 mm long and it can be reproduced as a 1-D domain with endpoints A and B, characterized by the spatial coordinate z (Fig. 2). In the considered infiltration process, the column is initially at atmospheric pressure with a uniform suction $s = 1.1$ kPa. This condition is simulated by setting an initial value of $p_g = 0$ kPa and $p_l = -1.1$ kPa throughout the whole domain. At time $t = 0$ s, infiltration is triggered through the application of a constant-head reservoir at the endpoint B, which corresponds to $p_l = 1.2$ kPa. No flow is allowed at the endpoint A. As for the air species, a Dirichlet boundary condition is applied on B, with a pressure equal to the corresponding p_l increased by the soil air-entry value AEV $= 0.1$ kPa (hence, $p_g = 1.3$ kPa). This constraint forces the suction in B to be at least equal to the AEV, thus allowing air to escape during the process. On A, a Neumann boundary condition forces the air flux to zero.

The model was integrated with the finite-element software Comsol Multiphysics®.
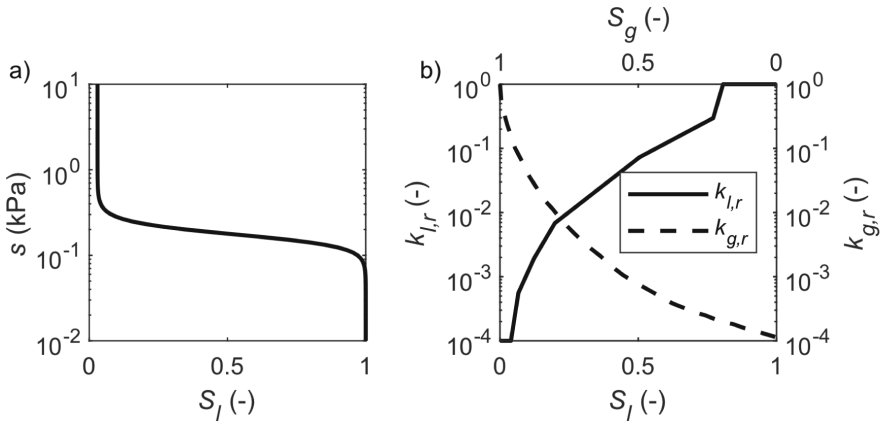

Fig. 1. a) Water retention curve of the soil; b) Relative permeability for the liquid and the gas phase, as a function of the liquid and the gas saturation degree (modified from [7]).
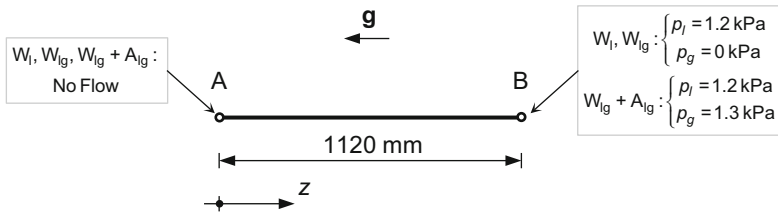
Fig. 2. Geometry of the modeled soil column, including boundary conditions. The vector **g** denotes the gravity acceleration.

4   Results and Discussion

Figure 3a–c show the simulated S_l profiles along column length at different times, for the three models. W_1 and W_{lg} models provide rather similar profiles, with a sharp wetting front for S_l increasing from the residual to the full saturated state. For comparison purposes, the wetting front was identified at any time by the point z_f, corresponding to the position where the derivative $\frac{\partial S_l}{\partial z}$ is maximum. Figure 3d reports the time evolution of z_f, which exhibits a linear trend over time and reaches endpoint A at about 400 s. At this time instant, the soil column achieves complete saturation. The strong agreement between W_1 and W_{lg} models is a consequence of the rather small variation of $p_g{}^w$ throughout the process (almost equal to $p^w_{g,sat}$ for all the time steps). As for the $W_{lg} + A_{lg}$ model, the shape and the evolution over time of the S_l profiles significantly changes compared with the models involving the water species only. On the one hand, the wetting front advances more slowly, and the time needed to reach endpoint A (900 s) is double with respect to
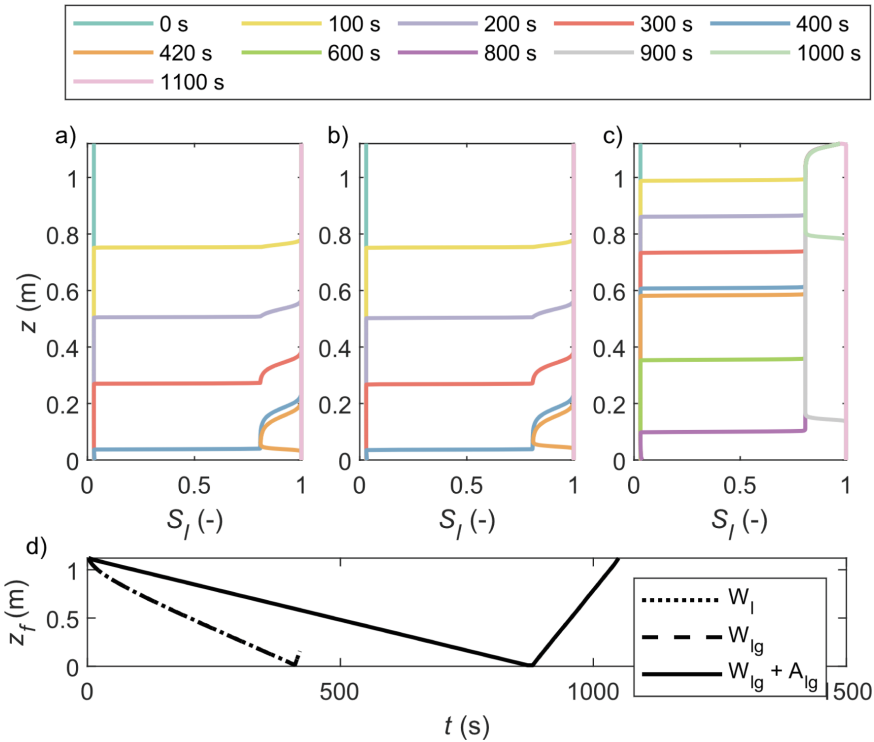
Fig. 3. a–c) Profiles of liquid-phase saturation degree S_l for different time instants, for a) "W_l" model, b) "W_{lg}" model and c) "$W_{lg} + A_{lg}$" model; d) Temporal evolution of the location of the wetting/saturation front, labeled as z_f.

the other cases. Besides, the region above the wetting front is still partially saturated, with $S_l \approx 0.8$. After $t = 900$ s, a saturation front gradually rises along the column, and the portion below it achieves $S_l = 1$. The saturation front proceeding from bottom to top is faster than the wetting front from top to bottom, and saturation completes at 1100 s.

The introduction in the model of the air species thus dramatically modifies the shape and the location of saturation isochrones. Indeed, the liquid water advancement is partially counterbalanced by an increase in the air pressure. Specifically, at each time instant, $p_g{}^a$ profiles exhibit a linear increase in the region above the wetting front, and it remains uniform below (Fig. 4). Indeed, the progressive saturation from one end of the model creates entrapped air, which reacts with an overpressure to the gradual confinement exerted by the advancing wetting front. The air pressure is maximum when the wetting front reaches the bottom of the column. When the wetting front reaches endpoint A, the air pressure gradually reduces from its maximum due a counterflow of air, thus allowing complete saturation of the column.
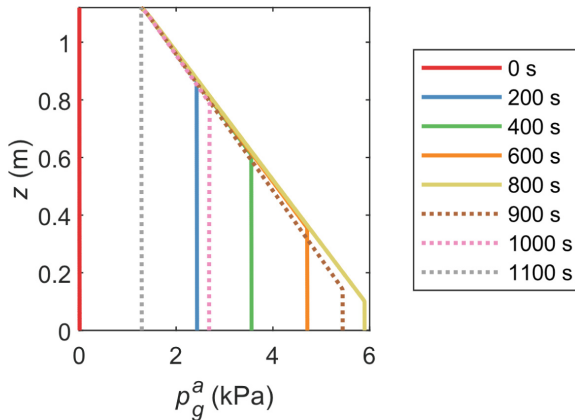
Fig. 4. Profiles of air gas pressure $p_g{}^a$ for different time instants. The dashed lines correspond to the final saturation stage, characterized by the ascent of the saturation front.

5 Conclusions

This contribution addressed the influence of accounting for the gas phase when modelling infiltration. A hydraulic model combining the mass transport of pore water and air was formulated, including both the liquid phase and the gas phase. The model was used to simulate infiltration along an initially dry soil column, considering the flow of liquid water only, the flux of liquid and water vapour, and the flow of both water and air.

Accounting for the presence of air significantly impacts the simulation results. Compared with the cases including only water mass balance, a relevant reduction in the infiltration rate is observed. Pore air partially hinders the water flow, resulting in a longer infiltration process and a slower build-up of pore water pressure. Instead, simulations accounting for water vapour do not substantially differ from those of the liquid-based model. This specific aspect may depend on the small suction range encompassed in the simulations (around 1 kPa), which entails an almost negligible variation of the vapour pressure.

These conclusions apply to the specific material and boundary conditions explored in the present work. Although the main features of the process might be expected to be the same also for fine soils, their relevance might be different depending on the water retention properties of the material. It shall be observed that, at *in-situ* conditions, infiltration is more realistically triggered by a precipitation rate rather than by an imposed water pressure at the ground surface. This different boundary condition might be expected to have a different impact of the air pressure build up, and therefore on infiltration and pressure isochrones.

References

1. Sánchez, M., Manzoli, O.L., Guimarães, L.J.: Modeling 3-D desiccation soil crack networks using a mesh fragmentation technique. Comput. Geotech. **62**, 27–39 (2014)

2. Musso, G., Vespo, V.S., Guida, G., Della Vecchia, G.: Hydro-mechanical behaviour of a cement–bentonite mixture along evaporation and water-uptake controlled paths. Geomech. Energy Environ. 100413 (2022). https://doi.org/10.1016/j.gete.2022.100413

3. Sitarenios, P., Casini, F., Askarinejad, A., Springman, S.: Hydro-mechanical analysis of a surficial landslide triggered by artificial rainfall: the Ruedlingen field experiment. Géotechnique **71**(2), 96–109 (2021)

4. Guida, G., Vespo, V.S., Musso, G., Della Vecchia, G.: The role of hydraulic and thermal properties of soil on evaporation: a numerical insight. Submitted to Environmental Geotechnics, under review (2023)

5. Richards, L.A.: Capillary conduction of liquids through porous mediums. Physics **1**, 318–333 (1931)

6. Siemens, G.A., Peters, S.B., Take, W.A.: Comparison of confined and unconfined infiltration in transparent porous media. Water Resour. Res. **49**(2), 851–863 (2013)

7. Siemens, G.A., Take, W.A., Peters, S.B.: Physical and numerical modeling of infiltration including consideration of the pore-air phase. Can. Geotech. J. **51**(12), 1475–1487 (2014)

8. McWhorter, D.B.: Infiltration affected by flow of air. PhD thesis, Colorado State University (1971)

9. Bear, J., Cheng, A.H.-D.: Modeling Groundwater Flow and Contaminant Transport, vol. 23. Springer, Dordrecht (2010). https://doi.org/10.1007/978-1-4020-6682-5

10. Kendall, C., Caldwell, E.A.: Fundamentals of isotope geochemistry. In: Isotope tracers in catchment hydrology, pp 51–86. Elsevier (1998)

11. Bear, J., Braester, C., Menier, P.C.: Effective and relative permeabilities of anisotropic porous-media. Transp. Porous Media **2**, 301–316 (1987)

12. Lai, S.H., Tiedje, J.M., Erickson, A.E.: In situ measurement of gas diffusion coefficient in soils. Soil Sci. Soc. Am. J. **40**(1), 3–6 (1976)

13. Kimball, B.A., Jackson, R.D., Reginatoe, R.J., Nakayama, F.S., Idso, S.B.: Comparison of field-measured and calculated soil-heat fluxes. Soil Sci. Soc. Am. J. **40**(1), 18–25 (1976)

14. Cussler, E.L.: Diffusion: Mass Transfer in Fluid Systems. Cambridge University Press, New York (1997)

15. Van Genuchten, M.T.: A closed-form equation for predicting the hydraulic conductivity of unsaturated soils. Soil Sci. Soc. Am. J. **44**(5), 892–898 (1980)